Ceramics International 46 (2020) 3028–3035

Contents lists available at ScienceDirect

Ceramics International

journal homepage: www.elsevier.com/locate/ceramint

Improved electrochemical performance of graphene oxide supported vanadomanganate (IV) nanohybrid electrode material for supercapacitors

Sparsha Kumari[a], Sukanya Maity[a], Anjana A. Vannathan[b], Debaprasad Shee[c], Partha Pratim Das[a,**], Sib Sankar Mal[b,*]

[a] Department of Physics, National Institute of Technology Karnataka, Surathkal, 575025, India
[b] Department of Chemistry, National Institute of Technology Karnataka, Surathkal, 575025, India
[c] Department of Chemical Engineering, Indian Institute of Technology Hyderabad, Kandi, Sangareddy, 502285, Telangana, India

ARTICLE INFO

Keywords:
Vanadomanganate
Graphene oxide
Supercapacitors
Cyclic voltammogram
Two-electrode system

ABSTRACT

Graphene oxide (GO)-supported polyoxometalates (POMs) have been considered as promising electrode materials for energy storage applications due to their ability to undergo fast and reversible redox reactions. Herein, vanadomanganate-GO composites ($K_7Mn^{IV}V_{13}O_{38}.18H_2O$-GO with 2:1 and 4:1 ratio) were investigated for use as potential electrode materials in supercapacitors (SCs). The $K_7Mn^{IV}V_{13}O_{38}.18H_2O$ (MnV_{13}) was synthesized and anchored on GO through electron transfer interaction and electrostatic interaction to make the composite electrodes for the present study. All synthesized electrode materials were fully characterized by various techniques, e.g., Fourier Transform Infrared (FTIR) Spectroscopy, Powder X-ray Diffraction (XRD), Scanning Electron Microscopy/Energy Dispersive X-ray Spectroscopy (SEM/EDS) and High Resolution-Transmission Electron Microscopy (HR-TEM). The electrochemical properties of MnV_{13}/GO composites with different MnV_{13}/GO ratios were investigated by two-electrode cyclic voltammetry (CV) and galvanostatic charge/discharge (GCD) in different electrolytes. The MnV_{13}/GO composite of ratio 2:1 in 1 M LiCl electrolyte and that of ratio 4:1 in 1 M Na_2SO_4 electrolyte showed significant specific capacitance values of 269.15 F/g and 387.02 F/g, respectively and energy density of 37.38 Wh/kg and 53.75 Wh/kg, respectively for a scan rate of 5 mV/s. Interestingly, the 1:1 (MnV_{13}/GO) composite in 1 M Na_2SO_4 and 1 M LiCl electrolytes showed very low specific capacitance values as the deposition of MnV_{13} on GO was not sufficient, as indicated by FTIR and SEM. Thus, it is evident that the specific capacitance value of these composite materials depends on the amount of MnV_{13} deposited on GO and these composite materials exhibit the potential to improve the performance of GO-based SCs.

1. Introduction

To meet the increasing demand for electrical energy in the modern world, there has been a need to produce clean energy and store a large amount of electrical energy in an eco-friendly way [1]. The large production of sustainable energy increases the importance of corresponding energy storage devices. Batteries and capacitors are the most commonly used energy storage devices with their own drawbacks [2]. Batteries store a large amount of energy but it takes several hours to charge up. In contrast, capacitors charge almost instantly but store only a small amount of energy. This aspect has pushed researchers towards building a different class of energy storage capacitive called "supercapacitors" (SCs). SCs are also known as ultracapacitors– thereby, bridging the gap between batteries and capacitors [2,3]. This electrochemical energy storage device stores electrical energy by converting chemical energy to electrical energy. Their charge/discharge time is significantly less compared to that of conventional batteries and they provide much higher energy density than normal capacitors [4–6]. In addition to the capability of SCs to store as much energy as batteries, the former can be fully recharged instantaneously [7]. Owing to their high-power density and long-cycle lifetime, SCs can be incorporated in portable electronic devices, memory backup systems, load leveling, hybrid electric vehicles, and many other electrical appliances [1,4,8–13].

SCs can store energy in two ways—one is electric double layer capacitance (EDLC) and other, is pseudocapacitance (faradic in nature). For the case of EDLC, carbon-based materials such as activated carbon (AC), carbon nanotubes(CNTs), carbon aerogels, etc. have been used as

* Corresponding author. Materials and Catalysis Lab, Department of Chemistry, National Institute of Technology Karnataka, Surathkal, India.
** Corresponding author.
E-mail addresses: daspm@nitk.edu.in (P.P. Das), malss@nitk.edu.in (S.S. Mal).

https://doi.org/10.1016/j.ceramint.2019.10.002
Received 30 August 2019; Received in revised form 30 September 2019; Accepted 1 October 2019
Available online 02 October 2019
0272-8842/

electrode material in SCs due to their low cost, availability in variety of forms (powders, fibres, aerogels, sheets, composites, etc.), controllable porosity and relatively inert electrochemical properties [3,9,11,14–17]. Those above-mentioned materials have low energy density and exhibit a limited capacitance, as the carbon-based materials have limited charge storage capability [4,7]. Although conducting polymers (e.g., polyanilines) can store charges in the electrical double layer and also show high pseudocapacitance, resulting in higher specific capacitance than that of carbon-based Electric Double Layer Capacitors (EDLCs) [3] they are brittle and weak in terms of mechanical strength, and therefore, SCs with these materials as electrode exhibit poor cyclic stability [7]. In order to enhance their cyclic stability, conducting polymers are complexed with carbon-based materials [7,18]. A high energy density can be achieved using a combination of carbon-based materials and pseudocapacitive materials such as transition metal oxides, electroconductive polymers (ECPs), polyoxometalates (POMs), among others [4,10,13,17].

Furthermore, ZnO/Graphene and MnO_2/GO nanocomposites have been employed as an electrode material for energy storage application which yielded specific capacitance values of 236 F/g and 192.7 F/g, respectively [19–21]. Efforts are on to search for new electrode materials to further improve the specific capacitance using GO as supporting material. In this regard, POMs have attracted a lot of attention as redox-active metal oxide electrode in energy storage devices [4,22].

POMs are transition metal-oxide inorganic water-soluble clusters with unique features, e.g., high thermal stability, electrical conductivities, and exhibit diverse properties such as catalytic activity and high stability in their redox states [23–29]. Due to the fast, reversible and stepwise multi-electron redox reactions, they exhibit a high capacity for energy storage applications [4,30,31]. Dissociation of ionic aggregates in aqueous solution and low specific surface area of POM ($< 10\,m^2\,g^{-1}$), make them necessary to be anchored on an insoluble solid matrix of the large surface area [8]. In this regard, carbon nanotubes and graphene can be considered as potential candidates as supporting solid matrix due to their considerably high surface area which enhances EDLC [8,32]. Composites of POMs with carbon nanotubes (CNTs) and graphene have been demonstrated to hold promise to meet the requirements of energy storage, electrocatalysis, sensor devices, etc. [33]. In addition, it was shown that the electronic properties of graphene can be modified by selecting the appropriate POMs [34].

There are very few reports available in the literature on POMs being used as supercapacitor electrodes [35–38]. It was in 1998, when A. Yamada from Japan, first demonstrated that POMs could be used as an electrode material for energy storage applications [5]. In Yamada's report, acid forms of POMs were employed as electrodes and a specific capacitance value of 112 F/g and an energy density of 36 J/g were obtained [5]. Furthermore, POMs were supported on different conducting polymers to make polymer-POM hybrid materials such as PAni/$H_3PMo_{12}O_{40}$ [39], PAni/PMo_{12} and PEDOT/PMo_{12} [40], which yielded specific capacitances of 120 F/g, 168 F/g, and 130 F/g, respectively. However, the combinations of POMs with carbon-based materials such as graphene, CNTs, ACs, GO, reduced GO (rGO), etc. have been subsequently reported with significant improvement in the specific capacitance and the energy density [8,41–46]. In 2014, H.-Y. Chen et al. studied the vanadium-based POM ($Na_6V_{10}O_{28}$) as an electrode material for SCs and obtained a fairly high capacitance value of 354 F/g [41]. Their work serves as an incentive for us to explore the use of vanadium-based POMs in order to improve overall performance in SCs. In 2014, Ni et al. showed that other compound MnV_{13} could also be used as a cathode material of lithium-ion battery applications [47]. H.-Y. Chen et al. observed that due to the availability of multiple oxidation states of vanadium metal (from V^{2+} to V^{5+}), V_2O_5 shows relatively higher specific capacitance [41] values. Similarly, manganese also shows multiple oxidation states (Mn^{2+} to Mn^{4+}) and MnO_2 on GO showed high specific capacitance [21]. Therefore, we believe that the combination of two different redox metal centers manganese-vanadium-containing POMs can serve as a promising electrode for SCs and thus, we choose MnV_{13} as an active redox electrode material for our current investigation [35,42].

In this report, we investigate for the first time the utilization of the GO supported vanadomanganate-containing POM (MnV_{13}) as electrode material in SC. Here, the different ratios of MnV_{13}/GO composites were synthesized and their electrochemical performances, such as cyclic voltammetry (CV) and galvanostatic charge/discharge (GCD) in Na_2SO_4 (1 M) and LiCl (1 M) electrolyte medium were investigated. We have chosen above mentioned two electrolytes for our current study to achieve high energy and power density. The demand for specific power and energy values determines the choice of the electrolyte used in our electrochemical analysis. Importantly, the stability and operating potential window of the electrolyte used to play a vital role in determining the performance metrics of a supercapacitor (SC). The potential window of acidic aqueous solutions is approximately 1V. This is because water splitting occurs above 1.23V. However, most of the SCs based on POM use acidic aqueous electrolytes like H_2SO_4, which limits the operating voltage of the SC.

Furthermore, H_2SO_4, being a strong acid, is highly corrosive in nature, which consequently limits practical application of the electrode materials. We also believe that there is a possibility that in strong acidic medium, POMs will leach out from the GO surface and which could further offer serious hindrance to the stability and durability of the electrode material. Therefore, neutral electrolyte such as Na_2SO_4 and LiCl are used in this work to achieve high energy and power density [41,48]. Also, we varied the amount of POM on the GO surface to realize the variation of pseudocapacitive properties.

2. Experimental section

2.1. Preparation of graphene oxide (GO)

We synthesized GO by exfoliation of graphite using the Modified Hummers Method as narrated in Refs. [49,50]. We took 2 g of graphite powder and sodium nitrate each followed by their mixing in 90 mL of 98% sulfuric acid at about 0 °C–5 °C with constant stirring on. After about 4 h, 12 g of potassium permanganate was slowly added to the suspended solution. The addition of potassium permanganate was precisely regulated to maintain the reaction temperature at less than 15 °C. Then 184 mL of distilled water was slowly added to the resulting compositions and stirred for approximately 2 h. The mixture temperature was then increased to 35 °C and stirred for 6 h. The resultant solution was then maintained at 98 °C in a reflux system for about 10–15 min. After 10 min the temperature was brought down to 30 °C to obtain a brown-colored solution. The reaction solution was kept at 25 °C for 2 h. The mixture was finally combined with 40 mL of hydrogen peroxide (30 w/v %) which resulted in a bright yellow solution. An equal amount of the prepared solution was then added to two separate beakers having 200 mL of water in it and stirred for 1 h. The solution was aged for around 3–4 h. The liquid was then filtered to obtain a mixture which was washed repeatedly by centrifugation with 10% hydrochloric acid followed by deionized water until a gel-like substance was obtained (pH neutral). Thus obtained GO gel was dried under vacuum at a temperature of 60 °C for 6 h to get GO powder.

2.2. Synthesis of potassium 13-vanadomanganate ($K_7Mn^{IV}V_{13}O_{38}.18\,H_2O$)

The synthesis of potassium 13-vanadomanganate was carried out using the method reported elsewhere [51]. A composition of 35.9 g of potassium metavanadate with around 900–1000 mL of hot water was prepared. We added, in order, 1 M nitric acid (20 mL), 20 mL of 1 M manganese(II) sulfate with 10.8 g of potassium peroxydisulfate to the as-prepared composition. The solution was then maintained at 80 °C and blended continuously ed while the mixture evaporated for a few hours. Initially, a brownish-red precipitate was seen to form which

again got dissolved in solution producing an orange-red and finally a brown-red colour solution. After 5–7 h, the volume of the solution mixture was decreased to 300 mL, and this compound solution then was filtered followed by addition of 40 mL of 1 M potassium acetate to it. After aging overnight, reddish-orange colored crystals were obtained and then washed with 0.5 M potassium acetate plus 0.5 M acetic acid. Then the solution was recrystallized with 0.5 M potassium acetate with 0.5 M acetic acid mixture and finally treated with ethanol and water mixture followed by 95% ethanol. After that, the crystals were air-dried and use for our studies.

2.3. Preparation of the composites

The three MnV_{13}/GO composites were synthesized using below-mentioned methods.

2.3.1. Preparation of MnV_{13}/GO composite of ratio 4:1

About 20 mg of GO was sonicated along with 20 mL of distilled water for 30 min. 80 mg of the synthesized MnV_{13} was dissolved in 10 mL of distilled water and then it was added dropwise to the GO solution. Then the mixture was again sonicated for 30 more min. The solution was then stirred for 24 h at room temperature and then dried in the hot-air oven at 60 °C. After air drying, the composites were collected and washed with distilled water several times and then air-dried.

2.3.2. Preparation of MnV_{13}/GO composite of ratio 2:1

This MnV_{13}/GO (2:1) composite was prepared using the method outlined above taking 40 mg of MnV_{13} to make the MnV_{13}/GO ratio 2:1.

2.3.3. Preparation of MnV_{13}/GO composite of ratio 1:1

This MnV_{13}/GO (1:1) composite was prepared using the method outlined above taking 20 mg of MnV_{13} to make the MnV_{13}/GO ratio 1:1.

2.4. Preparation of electrode

Two pieces of carbon cloth of dimension 2 cm × 2 cm were taken and their individual masses were measured separately. A 15 mg of the prepared composite was sonicated in 4 mL ethanol for 30 min and spread evenly over both the pieces of carbon cloth. The wet clothes were then dried for about an hour in the hot air oven at 60 °C and the mass of the composite-coated cloths were measured. A separator (filter paper) of dimension 2 cm × 2 cm was sandwiched between the two composite-coated cloths along with a few drops of the electrolyte (Na_2SO_4 or LiCl) spread over it. Then the two-electrode electrochemical measurements (IVIUM Vertex Galvanostat instrument) were performed with each of the cloths acting as an electrode.

3. Results and discussion

3.1. Material characterization of all MnV_{13}/GO composites

The GO and MnV_{13} were synthesized and characterized according to the procedures published elsewhere [49–51]. Fig. 1a shows the FTIR spectra (Bruker Alfa FTIR spectrometer) of all synthesized MnV_{13}/GO composites of different ratios as well as synthesized GO. The FTIR spectrum (Fig. 1a(i)) shows the characteristic absorption band of GO. The IR band at 1713 cm^{-1} is attributed to C═O, other IR bands at 1611, 1388, 1217, and 1043 cm^{-1} are assigned to C═C, C–O (carboxyl), C–O (epoxy), C–O (alkoxy), respectively [52]. The IR spectrum of MnV_{13} (Fig. S1, Supplementary Information) shows characteristic bands at around 963, 852, and 810 cm^{-1} attributed to the terminal V═O bonds and the V–O–V bridging bonds vibration. The band at 540 cm^{-1} designated to the Mn–O–V bridging bond vibration [47,53,54]. The composites of both the ratios showed all the characteristics peaks of GO and MnV_{13} as shown in Fig. 1b.

Fig. 2 shows the XRD pattern (Rigaku 600 mini flex X-ray diffractometer) of MnV_{13}/GO of ratio 2:1. The XRD pattern shows GO diffraction peak at 2θ of around 10° (0 0 2) and 42° (1 1 1) [55,56]. The diffraction peaks at 2θ = 15.533° (2 0 0), 20.258° (0 1 0), 26.268° (1 0 1) and at 31.138° (4 0 0) are characteristics peaks of the vanadium-oxygen crystal structure (from JCPDS data, card no. 00-001-0246) which confirms the presence of the materials (K, Mn. V, O) in crystalline form [57]. The XRD pattern of the composite of ratio 4:1 is shown in Fig. S2, where the presence of characteristic diffraction peaks of vanadium oxygen metal cluster is clearly indicated.

The surface morphology of all composites and GO along with EDS is shown in Fig. 3. The SEM image of GO (Fig. 3a) shows the random orientation and wavy appearance of exfoliated graphite oxide [58]. The SEM image of MnV_{13}/GO (2:1) in Fig. 3b shows the randomly oriented flakes type POM structures of about 89 nm in diameter and the corresponding EDS data confirms the presence of all elements in MnV_{13} on GO. On the other hand, in MnV_{13}/GO (4:1) (Fig. 3c), MnV_{13} is a flower-like structure with numerous “petals” of length of about 0.339 μm and width 0.136 μm, deposited on the surface of GO and it is uniformly distributed over GO surface and again the EDS data confirms the presence of all elements in MnV_{13} on GO.

The structural orientation and crystal planes of MnV_{13} were further investigated by HR-TEM. Fig. 4a shows the HR-TEM image of the composite of MnV_{13}/GO of ratio 4:1, which suggests the presence of ordered crystalline nano-rods of MnV_{13}. The d-spacing measured from the HR-TEM image (for the above-mentioned composite ratio) is 0.25 ± 0.2 nm. However, randomly oriented nano-rods of about 0.36 nm and 0.259 nm in diameter were observed for the composites of ratio 2:1 and 4:1 respectively as shown in Fig. 4 (insets).

3.2. Electrochemical performance of all MnV_{13}/GO composite electrodes

Two-electrode GCD and CV were performed (using IVIUM Vertex Galvanostat instrument) to examine the electrochemical performance of MnV_{13}/GO composites as an electrode material for SCs in 1 M Na_2SO_4 and 1 M LiCl electrolytes. The composites were prepared in appropriate ratios (as described in the experimental section) before it was employed for the study. The capacitance of all the composites was calculated using the area under the CV curve using the below equation.

$$C_S = \left(\int idV\right)/(2mv\Delta V)$$

where i, ΔV, v, and m represent the response current (A), the voltage window (V), the voltage scan rate (V/s), and the mass (g) of active material deposited on the electrode (on carbon clothe), respectively. Applying the above mathematical expression, the specific capacitance of composites MnV_{13}/GO (387.02 F/g, 4:1 ratio) in Na_2SO_4 electrolyte and MnV_{13}/GO (269.15 F/g, 2:1 ratio) in LiCl electrolyte at a scan rate of 5 mV/s can be calculated.

The electrochemical performances of all composites were investigated in two different electrolytes (Na_2SO_4 and LiCl) to explore the behavior of the electrodes. Fig. 5a and b show the CV curves of GO, MnV_{13}/GO (2:1) in LiCl electrolyte and MnV_{13}/GO (4:1) in Na_2SO_4 electrolyte. The curve of GO (Fig. 5a, inset) at a scan rate of 50 mV/s retain nearly rectangular shape indicating that there is no faradic process involved and that it exhibits almost pure electrochemical double-layer behavior [41,43]. In Na_2SO_4 electrolyte, the composite ratio of 4:1 shows specific capacitance of 387 F/g in 5 mV/s (Fig. 5b, Table 1), whereas in case of the composite ratio of 2:1 specific capacitance of 128.06 F/g in 5 mV/s (Fig. S3a, Table S1) was achieved. The low value of capacitance is attributed to the leaching of POM from the GO surface in Na_2SO_4 electrolyte medium, resulting in less storage energy of 17.79 Wh/kg for a scan rate of 5 mV/s. Therefore, the electrolyte was changed to LiCl and the analysis was carried out again for the ratio of 2:1, which resulted in specific capacitance value of 269.15 F/g for 5 mV/s scan rate (Fig. 5a, Table 2) and showed more storage energy of

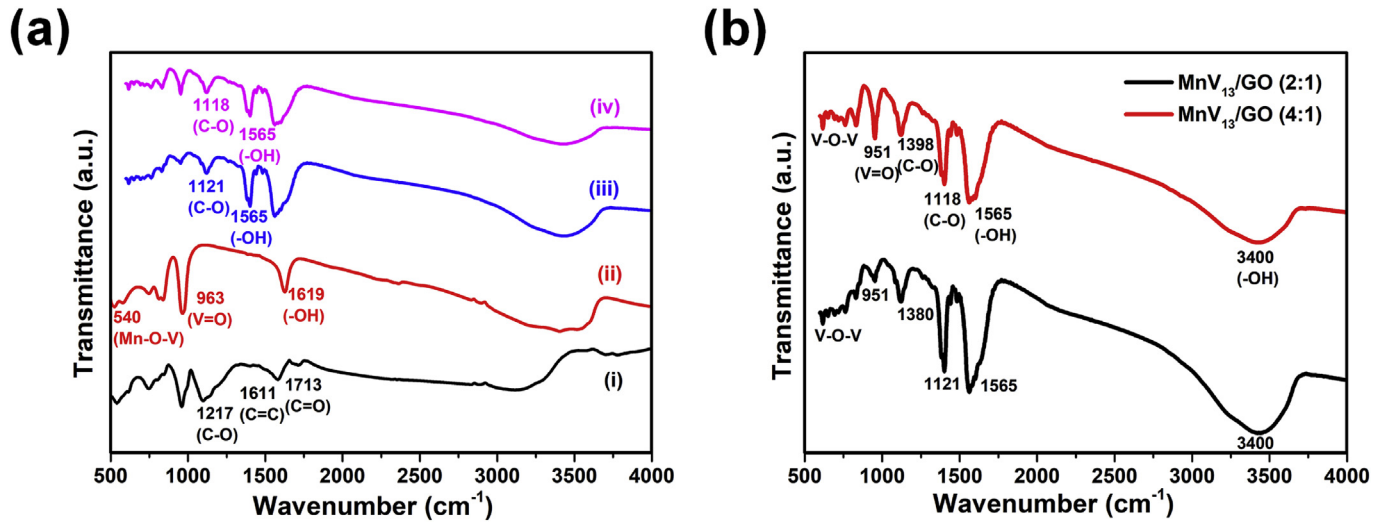

Fig. 1. FTIR spectrum of (**a**) (i) GO, (ii) MnV_{13}, (iii) MnV_{13}/GO (2:1), (iv) MnV_{13}/GO (4:1), (**b**) MnV_{13}/GO of ratio (2:1 and 4:1).

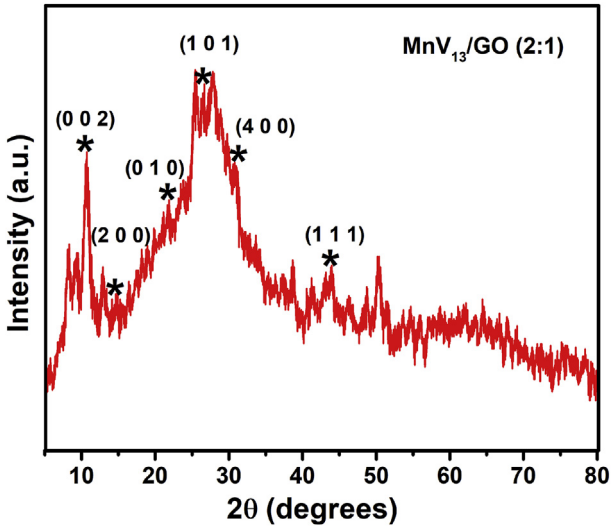

Fig. 2. XRD pattern of MnV_{13}/GO (2:1).

37.5 Wh/kg at the same scan rate (which is almost double the value of earlier). However, the composite of ratio 4:1 showed a moderate specific capacitance of 192.01 F/g in LiCl electrolyte for a scan rate of 5 mV/s (Fig. S3b, Table S2) and we believe this is due to the detachment of the POM layer (leaching of POM) from the GO surface in LiCl medium or due to the diffusion ion exchange phenomenon [41]. Furthermore, the composite of ratio 1:1 showed very little energy storage value in both the electrolytes (Figs. S3c and S3d, Tables S3 and S4). This may be due to a very little amount of POM deposited on GO matrix, which is confirmed by SEM images of the composite (Fig. S4). The potential range (0 to +1 V) was considered in the potential polarization range of working electrode and the available potential window was measured from the current values of reduction/oxidation of the supporting electrolyte [59,60]. The CV curves of MnV_{13}/GO (2:1) in 1 M LiCl electrolyte and MnV_{13}/GO (4:1) in1M Na_2SO_4 (Fig. 5a and b) electrolyte slightly deviate from the ideal rectangular shape indicating pseudocapacitive behavior (faradic process). This pseudocapacitance adds to the specific capacitance of GO, thus improving the specific capacitance of the MnV_{13}/GO hybrid electrode [4,41,43].

The MnV_{13}/GO hybrid electrodes showed much better specific capacitance and energy density values as compared to those of the pristine-GO electrode (Fig. 5b, inset). The MnV_{13}/GO composite of ratio 4:1 shows a high specific capacitance of 387.02 F/g and energy density of 53.75 Wh/kg at a scan rate of 5 mV/s in 1 M Na_2SO_4 electrolyte. We believe that the large specific capacitance and energy density values for the composite of ratio 4:1 are because of the more of quantity deposition of MnV_{13} on GO compared to that of ratio 2:1. This implies that the extent of redox-active POM deposition on GO matrix determines the specific capacitance as well as energy density values. Higher the amount of POM deposition on GO larger the electrical quantities provided POM does not leach out from GO support during the electrolysis process. These specific capacitance values were retained for more than 500 cycles.

In addition, we also examined galvanostatic charge/discharge (GCD) characteristics of both the composites of MnV_{13}/GO. The GCD curves of MnV_{13}/GO (2:1) at different areal current densities of 15 mA/cm^2, 30 mA/cm^2, and 45 mA/cm^2 are shown in Fig. 5c. The charge/discharge curves of MnV_{13}/GO (4:1) at current densities of 15 mA/cm^2 and 30 mA/cm^2 are shown in Fig. 5d. In the case of EDLC, the voltage varies linearly for the charge as well as for discharge, but for pseudocapacitance, the charge-discharge of the material varies with time (sec) exponentially. Therefore, all the charge/discharge curves are not strictly linear, indicating that the behavior of the MnV_{13}/GO hybrid electrodes is a combination of the double-layer capacitance contributed by GO and the pseudocapacitance attributed to MnV_{13} [41]. The specific capacitance, energy density, and power density were calculated for both the composites at various current densities (Tables S5 and S6 in SI units). The composite MnV_{13}/GO (2:1) showed specific capacitance, energy density and power density of 47.86 F/g, 6.65 Wh/kg and 40.91 kW/kg, respectively, at a current density of 45 mA/cm^2. Notably, Fig. 6 shows the comparison of the specific capacitance values obtained for GO, MnV_{13}/GO (2:1) in LiCl electrolyte and MnV_{13}/GO (4:1) in Na_2SO_4 electrolyte. It was evident from the GCD graphs that as we increase the areal current density, the potential window also increases resulting in higher capacitance and energy density but the voltage stability decreases as we decrease the discharge current. The electrochemical analysis of the MnV_{13}/GO hybrid material presented here shows that it can serve as a promising electrode material for SCs. We also found that by changing the concentration of the POM deposited on GO matrix and by choosing suitable electrolyte the electrochemical performance of SCs can further be improved.

4. Conclusions

In summary, different MnV_{13}/GO composite ratios were synthesized and then characterized using various structural as well as electrochemical analysis tools. Excellent interfacial contact and an increased

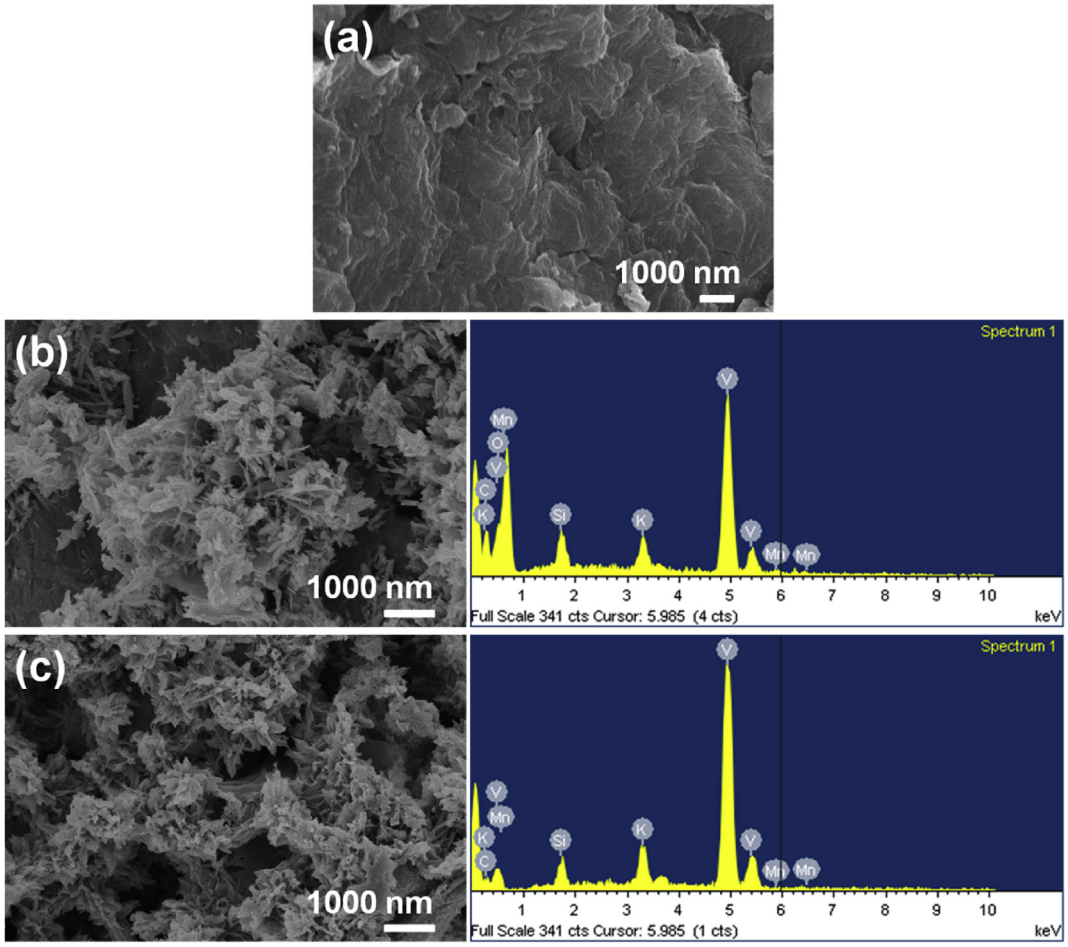

Fig. 3. (**a**) SEM image of GO, (**b**) SEM/EDS image of MnV_{13}/GO (2:1), (**c**) MnV_{13}/GO (4:1).

contact area between the POM and GO promote the quick charge transfer between POM and GO. The MnV_{13}/GO composite of ratio of 2:1 in LiCl electrolyte showed a specific capacitance of 269.15 F/g for a scan rate of 5 mV/s and a moderate energy density of 37.38 Wh/kg which gradually reduced to 4.30 Wh/kg with increasing scan rates and a high power density of 40.91 kW/kg at a current density of 45 mA/cm^2. MnV_{13}/GO (4:1) produced a specific capacitance of 387.02 F/g and energy density of 53.75 Wh/kg for a scan rate of 5 mV/s in Na_2SO_4 electrolyte. Specific capacitance values were found to vary with the choice of electrolyte used and also the contact area of composites. The CV and GCD curves indicate that the MnV_{13}/GO hybrid materials show a pseudocapacitive behavior and therefore, they can be used to improve the performance of the SCs. These results suggest that the MnV_{13}/GO composites potentially can serve as an effective electrode material for SCs.

Declaration of competing interest

The authors declare that they have no known competing financial interests or personal relationships that could have appeared to

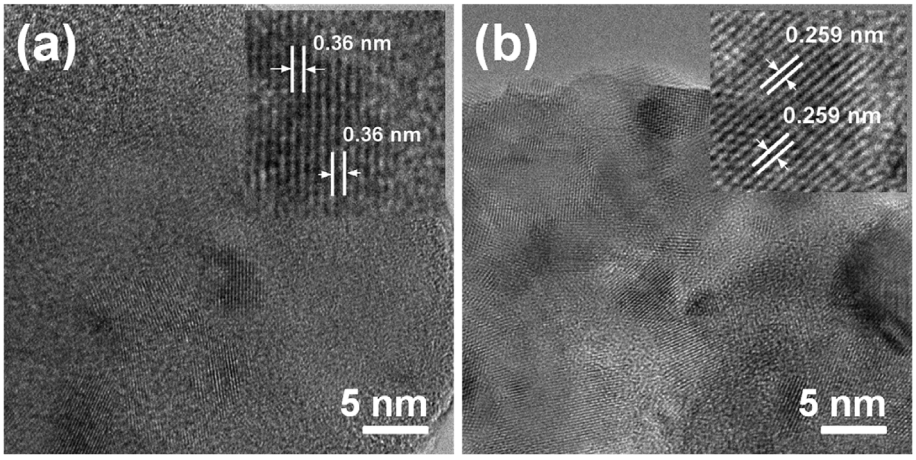

Fig. 4. HR-TEM image of (**a**) MnV_{13}/GO (2:1) and nanorods (inset), (**b**) MnV_{13}/GO (4:1) and nanorodes (inset).

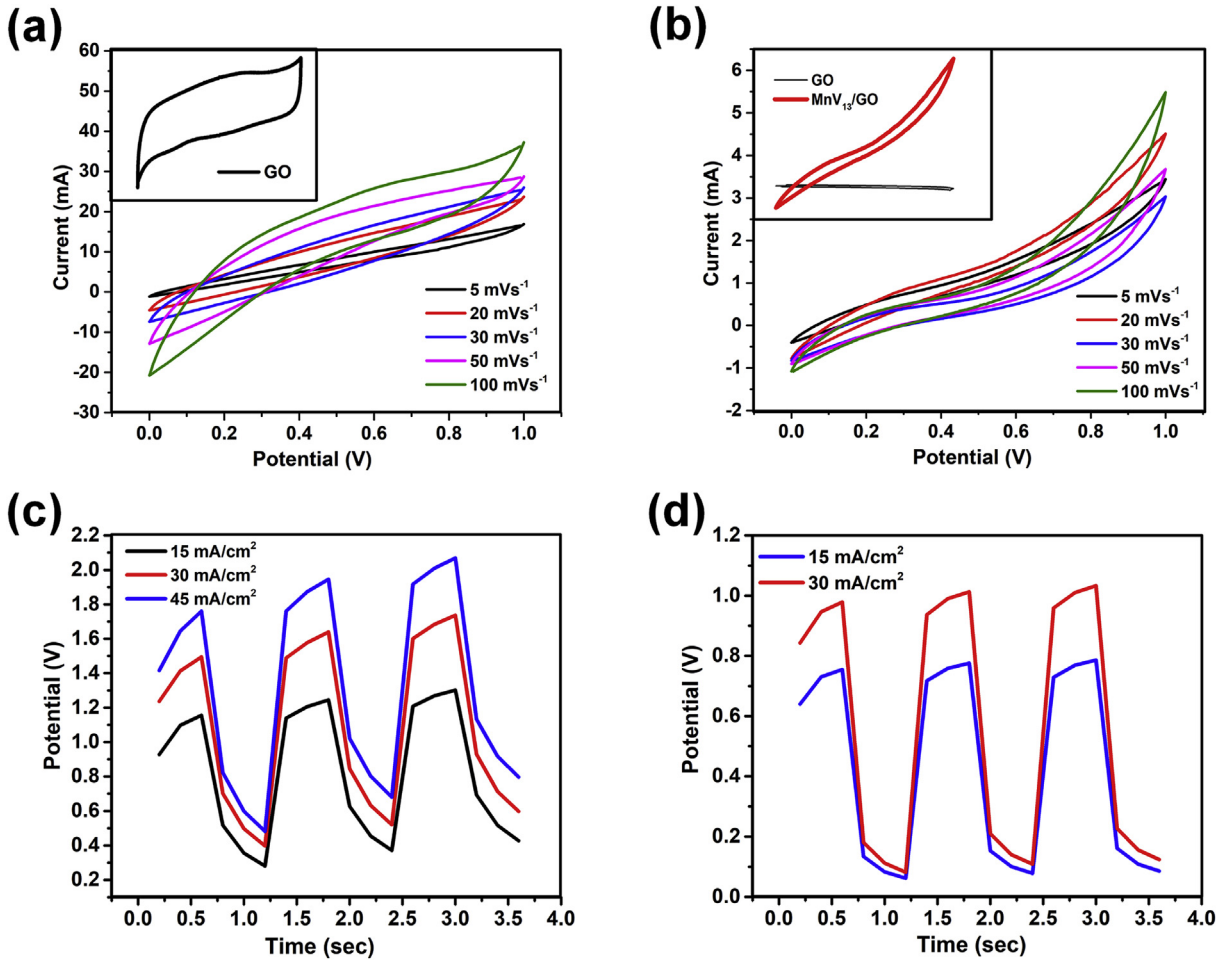

Fig. 5. Cyclic voltammogram of (**a**) MnV_{13}/GO (2:1) in 1 M LiCl and GO (inset), (**b**) MnV_{13}/GO (4:1) in 1 M Na_2SO_4 and comparison of CV curves of GO and MnV_{13}/GO (inset); Charge-discharge curves of (**c**) MnV_{13}/GO $_{13}$ (2:1) in 1 M LiCl, (**d**) MnV_{13}/GO (4:1) in 1 M Na_2SO_4 electrolyte solution.

Table 1
Specific capacitance and energy density values of MnV_{13}/GO (4:1) in 1 M Na_2SO_4 electrolyte.

Scan rate (mV s^{-1})	Specific capacitance (Fg^{-1})	Energy density (W h kg^{-1})
100	20.89	2.90
50	31.52	4.38
30	43.41	6.03
20	117.53	16.32
5	387.02	53.75

Table 2
Specific capacitance and energy density values of MnV_{13}/GO (2:1) in 1 M LiCl electrolyte.

Scan rate (mV s^{-1})	Specific capacitance (Fg^{-1})	Energy density (W h kg^{-1})
100	30.97	4.30
50	51.75	7.19
30	64.44	8.95
20	88.60	12.31
5	269.15	37.38

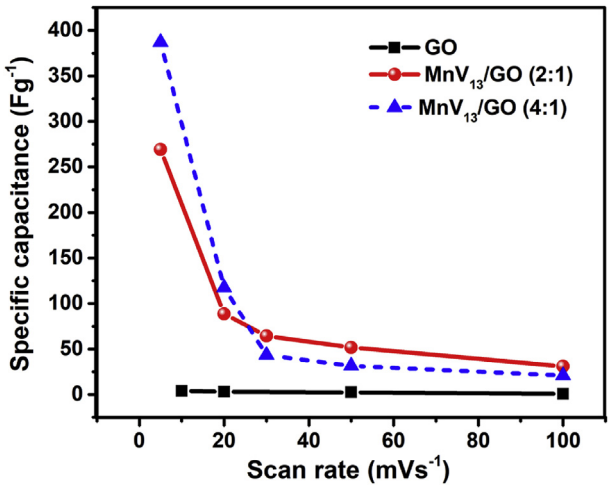

Fig. 6. Comparison of specific capacitances of GO, MnV_{13}/GO (2:1) and MnV_{13}/GO (4:1) at various scan rates.

influence the work reported in this paper.

Acknowledgments

Dr. S.S. Mal thank the Council of Scientific and Industrial Research (CSIR), India for financial support under schemes 01/(2906)/17/EMR-II. Dr. P. P. Das acknowledges Science and Engineering Research Board (SERB), Department of Science and Technology, Government of India for grant award EMR/2016/000808. AVV and SM thanks National Institute of Technology Karnataka, Surathkal for research scholarship.

Appendix A. Supplementary data

Supplementary data to this article can be found online at https://doi.org/10.1016/j.ceramint.2019.10.002.

References

[1] C. He, Z. Liu, H. Peng, Y. Yang, D. Shi, X. Xie, Room-temperature catalytic growth of hierarchical urchin-like MnO_2 spheres on graphene to achieve silver-doped nanocomposites with improved supercapacitor performance, Electrochim. Acta 222 (2016) 1393–1401.

[2] G.A. Snook, P. Kao, A.S. Best, Conducting-polymer-based supercapacitor devices and electrodes, J. Power Sources 196 (2011) 1–12.

[3] C. Peng, S. Zhang, D. Jewell, G.Z. Chen, Carbon nanotube and conducting polymer composites for supercapacitors, Prog. Nat. Sci. -Mater. Int. 18 (2008) 777–788.

[4] H.-Y. Chen, R. Al-Oweini, J.C. Friedl Lee, Y.L. Li, U. Kortz, U. Stimming, M. Srinivasan, A novel SWCNT-polyoxometalate nanohybrid material as an electrode for electrochemical supercapacitors, Nanoscale 7 (2015) 7934–7941.

[5] A. Yamada, J.B. Goodenough, Keggin type heteropolyacids as electrode materials for electrochemical supercapacitors, J. Electrochem. Soc. 145 (1998) 737–743.

[6] Y. Wang, Z. Shi, Y. Huang, Y. Ma, C. Wang, M. Chen, Y. Chen, Supercapacitor devices based on graphene materials, J. Phys. Chem. C 113 (2009) 13103–13107.

[7] C. Liu, Z. Yu, D. Neff, A. Zhamu, B.Z. Jang, Graphene-based supercapacitor with an ultrahigh energy density, Nano Lett. 10 (2010) 4863–4868.

[8] M. Yang, B.G. Choi, High-performance asymmetric supercapacitors based on polyoxometalate-graphene nanohybrids, Carbon Lett 18 (2016) 84–89.

[9] C. He, Y. Liang, P. Gao, L. Cheng, D. Shi, X. Xie, K.-Y. Li, Y. Yang, Bioinspired Co_3O_4/graphene layered composite films as self-supported electrodes for supercapacitors, Compos. B Eng. 121 (2017) 68–74.

[10] D.-Y. Kim, G.S. Ghodake, N.C. Maile, A.A. Kadam, D.S. Lee, V.J. Fulari, S.K. Shinde, Chemical synthesis of hierarchical $NiCo_2S_4$ nanosheets like nanostructure on flexible foil for a high performance supercapacitor, Sci. Rep. 7 (2017) 9764.

[11] Y. Ko, M. Kwon, W.K. Bae, B. Lee, S.W. Lee, J. Cho, Flexible supercapacitor electrodes based on real metal-like cellulose papers, Nat. Commun. 8 (2017) 536.

[12] X. Yang, H. Xia, Z. Liang, H. Li, H. Yu, Monodisperse carbon nanospheres with hierarchical porous structure as electrode material for supercapacitor, Nanoscale Res. Lett. 12 (2017) 550.

[13] H. Zhao, L. Liu, R. Vellacheri, Y. Lei, Recent advances in designing and fabricating self-supported nanoelectrodes for supercapacitors, Adv. Sci. 4 (2017) 1–34.

[14] L.L. Zhang, X.S. Zhao, Carbon-based materials as supercapacitor electrodes, Chem. Soc. Rev. 38 (2009) 2520–2531.

[15] J. Zhang, L.-B. Kong, B. Wang, Y.-C. Luo, L. Kang, In-situ electrochemical polymerization of multi-walled carbon nanotube/polyaniline composite films for electrochemical supercapacitors, Synth. Met. 159 (2009) 260–266.

[16] H. Wang, J. Lin, Z.X. Shen, Polyaniline (PANi) based electrode materials for energy storage and conversion, J. Sci. Adv. Mater. Devices. 1 (2016) 225–255.

[17] F. Razmjooei, K. Singh, T.H. Kang, N. Chaudhari, J. Yuan, J.-S. Yu, Urine to highly porous heteroatom-doped carbons for supercapacitor: a value added journey for human waste, Sci. Rep. 7 (2017) 10910.

[18] J. Zhang, X.S. Zhao, Conducting polymers directly coated on reduced graphene oxide sheets as high-performance supercapacitor electrodes, J. Phys. Chem. C 116 (2012) 5420–5426.

[19] Z. Li, Z. Zhou, G. Yun, K. Shi, X. Lv, B. Yang, High-performance solid-state supercapacitors based on graphene-ZnO hybrid nanocomposites, Nanoscale Res. Lett. 8 (2013) 473–481.

[20] E.R. Ezeigwe, M.T.T. Tan, P.S. Khiew, C.W. Siong, One-step green synthesis of graphene/ZnO nanocomposites for electrochemical capacitors, Ceram. Int. 41 (2015) 715–724.

[21] S. Chen, J. Zhu, X. Wu, Q. Han, X. Wang, Graphene oxide-MnO_2 nanocomposites for supercapacitors, ACS Nano 4 (2010) 2822–2830.

[22] D.P. Dubal, J. Suarez-Guevara, D. Tonti, E. Enciso, P. Gomez-Romero, A high voltage solid state symmetric supercapacitor based on graphene–polyoxometalate hybrid electrodes with a hydroquinone doped hybrid gel-electrolyte, J. Mater. Chem. A 3 (2015) 23483–23492.

[23] A. Müller, R. Sessoli, E. Krickemeyer, H. Bögge, J. Meyer, D. Gatteschi, L. Pardi, J. Westphal, K. Hovemeier, R. Rohlfing, J. Döring, F. Hellweg, C. Beugholt, M. Schmidtmann, Polyoxovanadates: high-nuclearity spin clusters with interesting Host − Guest systems and different electron populations. Synthesis, spin organization, magnetochemistry, and spectroscopic studies, Inorg. Chem. 36 (1997) 5239–5250.

[24] Y. Kim, S. Shanmugam, Polyoxometalate–reduced graphene oxide hybrid catalyst: synthesis, structure, and electrochemical properties, A*CS Appl. Mater. Interfaces* 5 (2013) 12197–12204.

[25] M.T. Pope, A. Müller, Polyoxometalate chemistry: an old field with new dimensions in several disciplines, Angew. Chem., Int. Ed. Engl. 30 (1991) 34–48.

[26] G. Wang, P. Ma, D. Zhang, J. Niu, J. Wang, Ni^{II}-embedded polyoxovanadate: synthesis, structure and magnetic properties, J. Alloy. Comp. 686 (2016) 1032–1036.

[27] S. Hartung, N. Bucher, H.-Y. Chen, R. Al-Oweini, S. Sreejith, P. Borah, Z. Yanli, U. Kortz, U. Stimming, H.E. Hoster, M. Srinivasan, Vanadium-based polyoxometalate as new material for sodium-ion battery anodes, J. Power Sources 288 (2015) 270–277.

[28] U. Jameel, M. Zhu, X. Chen, Z. Tong, Recent progress of synthesis and applications in polyoxometalate and nanogold hybrid materials, J. Mater. Sci. 51 (2016) 2181–2198.

[29] M. Ammam, Polyoxometalates: formation, structures, principal properties, main deposition methods and application in sensing, J. Mater. Chem. A. 1 (2013) 6291–6312.

[30] P.-E. Car, G.R. Patzke, The fascination of polyoxometalate chemistry, Inorga 3 (2015) 511–515.

[31] D. Xu, W.-L. Chen, J.-S. Li, X.-J. Sang, Y. Lu, Z.-M. Su, E.-B. Wang, The assembly of vanadium(IV)-substituted Keggin-type polyoxometalate/graphene nanocomposite and its application in photovoltaic system, J. Mater. Chem. A. 3 (2015) 10174–10178.

[32] R. Liu, G. Zhang, H. Cao, S. Zhang, Y. Xie, A. Haider, U. Kortz, B. Chen, N.S. Dalal, Y. Zhao, L. Zhi, C.-X. Wu, L.-K. Yan, Z. Su, B. Keita, Enhanced proton and electron reservoir abilities of polyoxometalate grafted on graphene for high-performance hydrogen evolution, Energy Environ. Sci. 9 (2016) 1012–1023.

[33] Y. Ji, L. Huang, J. Hu, C. Streb, Y.-F. Song, Polyoxometalate-functionalized nanocarbon materials for energy conversion, energy storage and sensor systems, Energy Environ. Sci. 8 (2015) 776–789.

[34] J.-P. Tessonnier, S. Goubert-Renaudin, S. Alia, Y. Yan, M.A. Barteau, Structure, stability, and electronic interactions of polyoxometalates on functionalized graphene sheets, Langmuir 29 (2013) 393–402.

[35] G. Wee, H.Z. Soh, Y.L. Cheah, S.G. Mhaisalkar, M. Srinivasan, Synthesis and electrochemical properties of electrospun V_2O_5 nanofibers as supercapacitor electrodes, J. Mater. Chem. 20 (2010) 6720–6725.

[36] J. Zheng, Y. Zhang, T. Hu, T. Lv, C. Meng, New strategy for the morphology-controlled synthesis of V_2O_5 microcrystals with enhanced capacitance as battery-type supercapacitor electrodes, Cryst. Growth Des. 18 (2018) 5365–5376.

[37] J.-J. Chen, J.-C. Ye, X.-G. Zhang, M.D. Symes, S.-C. Fan, D.-L. Long, M.-S. Zheng, D.-Y. Wu, L. Cronin, Q.-F. Dong, Design and performance of rechargeable sodium ion batteries, and symmetrical Li-ion batteries with supercapacitor-like power density based upon polyoxovanadates, Adv. Energy Mater. 8 (2018) 1701021.

[38] J.L. Gunjakar, A.I. Inamdar, B. Hou, S. Cha, S.M. Pawar, A.A.A. Talha, H.S. Chavan, J. Kim, S. Cho, S. Lee, Y. Jo, H. Kim, H. Im, Direct growth of 2D nickel hydroxide nanosheets intercalated with polyoxovanadate anions as a binder-free supercapacitor electrode, Nanoscale 10 (2018) 8953–8961.

[39] A.K. Cuentas-Gallegos, M. Lira-Cantú, N. Casañ-Pastor, P. Gómez-Romero, Nanocomposite hybrid molecular materials for application in solid-state electrochemical supercapacitors, Adv. Funct. Mater. 15 (2015) 1125–1133.

[40] J. Vaillant, M. Lira-Cantu, K. Cuentas-Gallegos, N. Casañ-Pastor, P. Gómez-Romero, Chemical synthesis of hybrid materials based on PAni and PEDOT with polyoxometalates for electrochemical supercapacitors, Prog. Solid State Chem. 34 (2006) 147–159.

[41] H.-Y. Chen, G. Wee, R. Al-Oweini, J. Friedl, K.S. Tan, Y. Wang, C.L. Wong, U. Kortz, U. Stimming, M. Srinivasan, A polyoxovanadate as an advanced electrode material for supercapacitors, ChemPhysChem 15 (2014) 2162–2169.

[42] Z. Chen, V. Augustyn, J. Wen, Y. Zhang, M. Shen, B. Dunn, Y. Lu, High-performance supercapacitors based on intertwined CNT/V_2O_5 nanowire, Nanocomposites Adv. Mater. 23 (2011) 791–795.

[43] A.K. Cuentas-Gallegos, R. Martínez-Rosales, M. Baibarac, P. Gómez-Romero, M.E. Rincón, Electrochemical supercapacitors based on novel hybrid materials made of carbon nanotubes and polyoxometalates, Electrochem. Commun. 9 (2007) 2088–2092.

[44] V. Ruiz, J. Suárez-Guevara, P. Gomez-Romero, Hybrid electrodes based on polyoxometalate–carbon materials for electrochemical supercapacitors, Electrochem. Commun. 24 (2012) 35–38.

[45] Z. Khan, S. Bhattu, S. Haram, D. Khushalani, SWCNT/$BiVO_4$ composites as anode materials for supercapacitor application, RSC Adv. 4 (2014) 17378–17381.

[46] J. Wang, X. Wang, D. Gu, C. Liu, L. Shen, Synthesis and characterization of polyoxometalate/graphene oxide nanocomposites for supercapacitor, Ceram. Int. 44 (2018) 17492–17498.

[47] E. Ni, S. Uematsu, N. Sonoyama, Lithium intercalation into the polyoxovanadate $K_7MnV_{13}O_{38}$ as cathode material of lithium ion batteries, Solid State Ion. 268 (2014) 222–225.

[48] E. Frackowiak, F. Beguin, Carbon materials for the electrochemical storage of energy in capacitors, Carbon 39 (2001) 937–950 Chen, H.-Y.; Wee, G.; Al- Oweini, R.; Friedl, J.; Tan, K. S.; Wang, Y.; Wong, C. L.; Kortz, U.; Stimming, U.; Srinivasan, M. A Polyoxovanadate as Advanced Electrode Material for SupercapacitorsChemPhysChem. 2014, 15, 2162-2169.

[49] D.C. Marcano, D.V. Kosynkin, J.M. Berlin, A. Sinitskii, Z. Sun, A. Slesarev, L.B. Alemany, W. Lu, J.M. Tour, Improved synthesis of graphene oxide, ACS Nano 4 (2010) 4806–4814.

[50] T. Chen, B. Zeng, J.L. Liu, J.H. Dong, X.Q. Liu, Z. Wu, X.Z. Yang, Z.M. Li, High throughput exfoliation of graphene oxide from expanded graphite with assistance of strong oxidant in modified Hummers method, J. Phys. Conf. Ser. 188 (2009) 012051.

[51] C.M. Flynn, M.T. Pope, 1:13 Heteropolyvanadates of manganese(IV) and nickel(IV), J. Am. Chem. Soc. 92 (1970) 85–90.

[52] D. Chen, H. Feng, J. Li, Graphene oxide: preparation, functionalization, and electrochemical applications, Chem. Rev. 112 (2012) 6027–6053.

[53] S. Chakrabarty, R. Banerjee, Kinetics and mechanism of oxidation of 2-mercaptoethanol by the heteropolyoxovanadate $[MnV_{13}O_{38}]^{7-}$, Int. J. Chem. Kinet. 47 (2015) 13–18.

[54] A.A. Davydov, O.I. Goncharova, Use of IR spectroscopy in studies of catalysts based on molybdenum heteropoly compounds supported on oxides, Russ. Chem. Rev. 62 (1993) 105.

[55] L. Stobinski, B. Lesiak, A. Malolepszy, M. Mazurkiewicz, B. Mierzwa, J. Zemek, P. Jiricek, I. Bieloshapka, Graphene oxide and reduced graphene oxide studied by

the XRD, TEM and electron spectroscopy methods, J. Electron. Spectrosc. Relat. Phenom. 195 (2014) 145–154.
[56] B. Zhao, P. Liu, Y. Jiang, D. Pan, H. Tao, J. Song, T. Fang, W. Xu, Supercapacitor performances of thermally reduced graphene oxide, J. Power Sources 198 (2012) 423–427.
[57] J.D. Hanawalt, H.W. Rinn, L.K. Frevel, Chemical analysis by X-ray diffraction, Ind. Eng. Chem. Anal. Ed. 10 (1938) 457–512, https://doi.org/10.1021/ac50125a001.
[58] S. Stankovich, D.A. Dikin, R.D. Piner, K.A. Kohlhaas, A. Kleinhammes, Y. Jia, Y. Wu, S.T. Nguyen, R.S. Ruoff, Synthesis of graphene-based nanosheets via chemical reduction of exfoliated graphite oxide, Carbon 45 (2007) 1558–1565.
[59] F. Scholz, Electroanalytical Methods: Guide to Experiments and Applications, Springer, 2013.
[60] N. Elgrishi, K.J. Rountree, B.D. McCarthy, E.S. Rountree, T.T. Eisenhart, J.L. Dempsey, A practical beginner's guide to cyclic voltammetry, J. Chem. Educ. 95 (2018) 197–206.